



# Modelling of Multi-Phase Interleaved based Universal Charging Port for Electric Vehicles

Vageesh Amoriya<sup>1</sup> · Rajeev Kumar Chauhan<sup>1</sup> · Shrestha Mittal<sup>1</sup> · Shivam Sharma<sup>1</sup> · Kalpana Chauhan<sup>1,2</sup> · Haiyu Li<sup>1,3</sup>

Received: 26 April 2023 / Accepted: 2 February 2024

© The Author(s), under exclusive licence to Springer Nature Singapore Pte Ltd. 2024

## Abstract

This paper presents the evolution of a multi-phase interleaved universal charging port to interconnect electric vehicles with the grid. The proposed charger facilitates users to charge their electric vehicles in any one of four modes: slow, medium, fast, and ultra-fast, optimizing the charging time and electricity bill. It can operate in manual as well as automatic mode. In manual mode, it charges the vehicle at a fixed rate, while in automatic mode, it automatically adjusts the charging rates based on the stress level of the grid. The proposed design offers economic gains to utility companies and electric vehicle users by allowing them to vary the charging rate during peak and off-peak hours. By charging during off-peak hours, users can take advantage of lower electricity rates and reduce their overall energy costs. Additionally, this design provides ancillary services to utility companies by allowing them to vary the charging rates of electric vehicles during peak hours. The performance of the proposed charger with the control algorithm is verified by simulation on MATLAB Simulink.

**Keywords** Electric Vehicle · Buck Converter · Multi-Phase Converter · Priority Encoder · Interleaved Converter Topology · Stability Boundary Locus

## Nomenclature

$V_{IN}$	Input voltage
$V_O$	Output voltage
$r_{sw}$	Switch ON Resistance
$r_L$	Equivalent series resistance of Inductor
$r_C$	Equivalent series resistance of Capacitor
$r$	Load resistance
$L$	Inductor
$C$	Capacitor
$r_D$	Forward Resistance of diode
$V_F$	Forward voltage of diode
$V_C$	Voltage drop across capacitor
$V_L$	Voltage drop across inductor

$F_{sw}$	Switching frequency across inductor
CCS	Combined Charging System

## Introduction

Governments are concerned about environmental pollution caused by fossil fuels, especially from conventional IC engine vehicles [1, 2]. Because of the continuous environmental catastrophe, the global economy is transforming its energy focus from a fossil fuel-based economy to one focused on renewable energy [3, 4]. To reduce range anxiety and motivate users to adopt EVs, charging station infrastructure is necessary Fig. 1. At present there are various charging standards adopted globally by different automobile companies and at the same time Government of Indian has also come up with its own charging standards [5, 6] (Refer Table 1). Currently the charging ports that are available are capable of charging vehicles efficiently but at a fixed charging level [7].

Charging at public charging stations is more expensive compared to domestic charging solutions, although they offer DC fast charging. Due to cost-effectiveness, users mostly prefer domestic chargers, even though their charging speed is slower. To increase the charging speed, users need to obtain a higher load rating for their connection, which

✉ Rajeev Kumar Chauhan  
rajeevchr\_nitj@yahoo.com

<sup>1</sup> Department of Electrical Engineering, Dayalbagh Educational Institute (Deemed to be University), Agra, Uttar Pradesh 282005, India

<sup>2</sup> Department of Electrical Engineering, School of Engineering and Technology, Central University of Haryana Mahendragarh, Haryana-123029, India

<sup>3</sup> Department of Electrical and Electronic Engineering, The University of Manchester, Oxford Rd, Manchester M13 9PL, UK

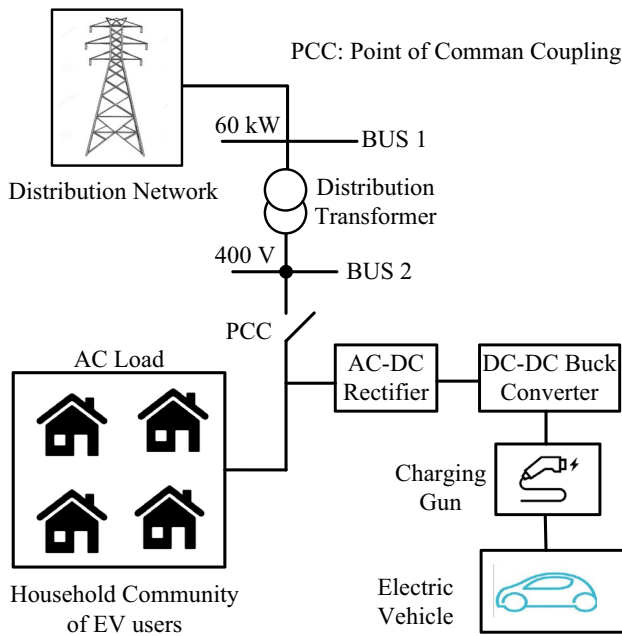


Fig. 1 System Architecture of EV Charging Station

Table 1 Popular Charging Standards

Type of Charging Gun	Specifications
TESLA-AC	Single Phase, 240V, 63A, 22-43 kW
CCS-Type 1: DC	50-1000 V, 80A, 80 kW
CCS-Type 2: DC	50-1000V, 400A, 400 kW
TYPE 1-AC (SAEJ1772)	Single Phase, 250 V, 32 A, 6.6 kW
Bharat Charger CG: DC	48-120 V, 200 A, 15 kW
Type 2: AC (CCS-TYPE 2:AC)	Single Phase, 480 V, 63A, 4 kW
Tata Nexon Type 1: AC	230 V, 15A, 3.2 kW
Tata Nexon Type 3: DC	150-750V, 100A, 30 kW
MG ZS EV: CCS-Type 1: DC	Three Phase AC, 50-500V, 50 kW
CCS-Type 2: AC	Single Phase, 480 V, 63A, 44 kW

is not always feasible. The current charging solutions limit user flexibility, as they only provide charging at a fixed rate. Electric vehicles can add to the grid's load and exceeding the charger's rating could lead to grid instability. Bidirectional charging can be used to address this issue by using the stored charge in the vehicle's battery to maintain power across the grid, especially when there is insufficient power to fulfil load requirements. [8].

In this paper we have proposed an EV charging solution at community level which can support variable charging rate based on availability of power across the grid. To evaluate the system with great accuracy and precision, we offer a suggestion for setting up an EV charging station for a neighborhood of different users. Actual load data from a neighborhood of four households has been considered. [9].

The proposed algorithm will estimate the power requirement at user end and based on availability of remaining power across the grid the EV charger can be used at that level in order to maintain grid stability because if every user opt for charger with high rating at same electric connection, then it will lead to grid failure and switching for electric connection with high rating is not an economically viable solution because it will increase the overall electricity bill. DC-DC Converter is a major component for various applications in renewable energy systems, battery energy storage, electric vehicles, hybrid-electric vehicles, and industrial automation. Apart from all these applications DC-DC Buck converter is a crucial component for electric vehicle charging stations because it regulates output voltage across low voltage bus to charge the vehicle's battery [10–12].

For DC-DC Conversion among various topologies of converters interleaved buck converter is incorporated to fulfil the objective of step down the DC voltage by adjusting the duty cycle applied to switching devices (in most cases MOSFET'S and IGBT'S) and increase the output current to drive the load [13]. Interleaving is technique where multiple switches are connected in parallel connection and operated with relative phase shift to increase the effective pulse frequency. In simple terms main advantage of interleaving topology is that it improves the system efficiency by splitting output current in multiple stages thus reducing  $I^2R$  and inductor AC losses, output ripple voltage and current which provides constant current for proper and safe charging of EV battery pack. Multi-Phase Interleaved power converters are highly beneficial for high performance electrical equipment due to low sizing of components which leads to reduction in electromagnetic emission and increase in transient response of the system [14, 15]. The mathematical modelling and controller design to maintain the required output voltage is an important aspect of DC-DC converter [16] as it helps to design a proper control scheme for the required system. Techniques such as state space averaging [17] are also used for this purpose. It is usually needed in DC-DC converters that output voltage achieved should be consistent despite variations in source voltage, load current, and component parameters. For improved stability and quick transient reaction of the system, various control approaches such fuzzy logic controller, artificial neural network (ANN), PID controller, and PI controller are applied [18, 19]. In this paper for experimental analysis specification of CCS (Combined Charging System) Type 1: DC fast charger with power rating 48 kW have been considered. It operates at input of 480V, three phase AC and consists of two stages i.e., AC-DC and DC-DC Conversion. Fast charging of EV batteries requires high current, but it leads to problem such as high distortion, low power factor and voltage drop at DC Link capacitor. To tackle the above problem of AC-DC rectification Vienna

rectifier is used in place of conventional diode-based rectifier. To reduce the cost of filter capacitor delta connected Vienna rectifier is recommended [20, 21].

As discussed above a buck converter is used to step down the DC voltage whereas The main purpose to implement multi-Phase buck converter over single phase buck converter is that single-phase buck controllers work effectively for low-voltage converter applications with current rating of up to 25 A (Approx.), but at higher current rating Power dissipation and overall efficiency tends to decrease, the issue to maintain high current rating with increase in overall efficiency can be maintained using multi-phase buck converter [22]. To regulate the output of the proposed system we have utilized a classical control approach with the help of PI Controller. To tune the designed controller, we have made use of graphical based approach depending on  $K_p$  and  $K_i$  at specified phase margin [23, 24].

The current research on the topic of multi-phase interleaved universal charging port for electric vehicles has identified several important findings. However, there is a gap in the literature when it comes to rate of charging of domestic chargers due to economic viability. In this paper, we aim to address this gap by developing a control strategy for designed multiphase interleaved buck converter to provide EV charging solution at community level which can support variable charging rate based on availability of power across the grid.

Specifically, our contributions are:

- The present solutions available do not provide a degree of freedom to the user because chargers available are only able to provide charging at fixed rate. we offer a suggestion for setting up an EV charging station for a neighbourhood of different users because if every user opt for charger with high rating at same electric connection, then it will lead to grid failure.
- The proposed algorithm will estimate the power requirement at user end and based on availability of remaining power across the grid the EV charger can be used at that level to maintain grid stability.
- To tune the controller with better visualization of stability and performance trade-offs we made use of stability boundary locus technique. The SBL technique is based on rigorous mathematical analysis of the system's open-loop transfer function, and it provides a clear understanding of the system's stability margins and performance limitations. These contributions build on the existing literature provides new insights on various topologies of DC-DC converters which can be proved useful to fulfil the concept of universal charging, methodologies to tune the designed controller with better stability and performance, ways to develop control technique to provide variable charging rate [25, 26] as per user's requirements. Overall, our

paper aims to advance the field by promoting fast, cost and energy efficient charging of EVs at domestic level.

The proposed multi-phase interleaved universal charging port for electric vehicles presents a range of advantages centered on its dynamic charging rate adjustment capabilities. One key benefit is user prioritization, allowing users to tailor charging rates according to their preferences and urgency. For instance, individuals in need of a quick charge for immediate use can opt for a fast or ultra-fast charging rate. The system also excels in grid load management by intelligently adapting the charging rate to the current load on the electric grid. During periods of low demand or surplus energy generation, the charger can operate at an accelerated rate, contributing to grid stability. Load balancing is another advantage, as the system slows down charging during high-demand periods, preventing grid congestion and ensuring a more stable electrical infrastructure. Integration with renewable energy sources is facilitated by the ability to charge at a faster rate during periods of surplus energy, aligning with the intermittent nature of sources like solar and wind. Support for public utility is inherent in the charger's responsiveness to grid conditions, enhancing overall reliability and efficiency and reducing the risk of blackouts or overloads. The system's flexibility and adaptability, operating in different modes based on external conditions, contribute to handling variations in electricity demand and supply effectively.

This Paper is organized as follows, in section II of this paper transfer function of non-ideal single stage buck converter is estimated using the concept of mathematical modelling followed by the frequency response analysis of designed converter using Bode Plot. To improve the dynamics or the transient response of the designed system to be stable PI Controller is tuned using stability boundary locus approach.

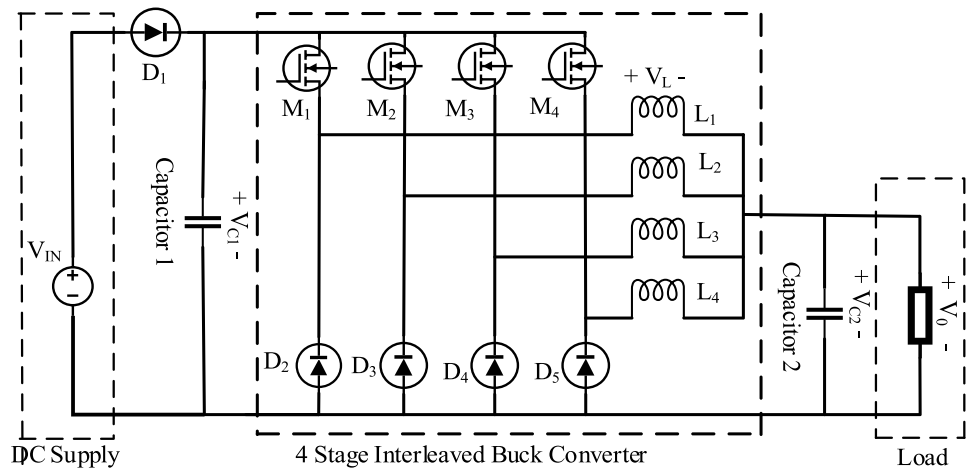
Section III provides a logical analysis of the given algorithm through implementation of priority encoder based combinational logic along with control technique is realized to achieve the output charging rate based on the remaining power available across the grid. Section IV presents simulation and experimental results to validate the proposed hypotheses and section V gives some concluding remarks.

## Methodology

A four-stage interleaved buck converter topology is shown in Fig. 2. It consists of four semiconductor switches i.e., MOSFETs ( $M_1$ ,  $M_2$ ,  $M_3$ , and  $M_4$ ), protection diode ( $D_1$ ) to prevent reverse flow of current, inductor ( $L_1$ ,  $L_2$ ,  $L_3$ , and  $L_4$ ), freewheeling diode ( $D_2$ ,  $D_3$ ,  $D_4$ , and  $D_5$ ), output filter capacitor ( $C_1$ ), load resistance ( $R$ ) and DC supply voltage ( $V_{IN}$ ).

The inductor windings  $L_1$ ,  $L_2$ ,  $L_3$  and  $L_4$  are directly connected from the Voltage source. There are four diodes

**Fig. 2** Multi-Phase Interleaved Converter Topology for Priority Based Charging



in the circuit, three semiconductor switches (MOSFET) and an output capacitor (C), are also included in the converter architecture and are connected across the Resistive load. In order to free wheel the leakage current through the switch, a diode is also merged to the switches to free-wheel the leakage current. In this study, a multi-device interleaved DC-DC buck converter has been designed and tested, comprising four identical converter phases. Each phase includes a set of components, namely MOSFETs ( $M_1, M_2, M_3,$  and  $M_4$ ), a diode ( $D_2, D_3, D_4,$  and  $D_5$ ), an inductor ( $L_1, L_2, L_3,$  and  $L_4$ ), and the load as shown in Fig. 2. The operation of MOSFET switches  $M_1, M_2, M_3,$  and  $M_4$  is orchestrated to be out of phase with each other. Importantly, the switches are activated based on current requirements, control circuit is dynamically adjusting the number of switches that are ON. If the current requirement increases, additional switches will be turned ON, optimizing the converter's performance. This interleaved operation effectively mitigates input and output ripple currents, while a control circuit also adjusts the duty cycles of the switches ( $M_1, M_2, M_3,$  and  $M_4$ ) in response to output voltage and load conditions. The interleaved nature of

the operation not only minimizes ripple effects but also distributes the load, thereby reducing stress on individual components and enhancing overall efficiency.

### Analysis Of Buck Converter

A DC-DC buck converter is a type of power electronic circuit that reduces the magnitude of an applied direct current voltage. . As illustrated in Fig. 3, the buck converter circuit comprises of several elements such as an inductor, a semiconductor switch (MOSFET or IGBT), a power diode, and a filter capacitor. *Let us assume the following parameter of Buck converter:*  $V_{IN} = 480$ -volt, power = 12 kW,  $V_o = 300$  volt, switching frequency ( $F_{sw}$ ) = 25 kHz, then

$$\frac{\Delta V_o}{V_o} = 1\% = 0.01 \tag{1}$$

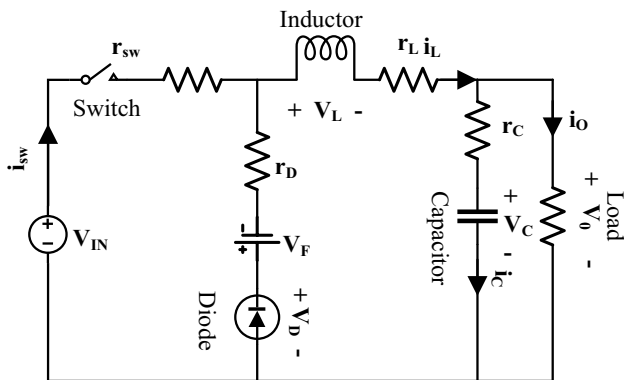


**Fig. 3** Schematic of Non-Ideal buck converter

**Table 2** Simulation parameters of four stage interleaved buck converter

Parameters	Specifications
Input Voltage ( $V_{IN}$ )	480 volts
Out Voltage ( $V_O$ )	300 volts
Power Rating of 4 stage Interleaved Converter	48 kW
Power Rating of single buck converter	12 kW
$F_{sw}$	25 kHz
R	1.875-7.5 $\Omega$
$C/r_C$	133 $\mu$ F/0.3 $\Omega$
$L/r_L$	56.25 $\mu$ H/0.18 $\Omega$
$r_{sw}$	0.01 $\Omega$
$V_F$	0.8 volt
EV Battery Nominal Voltage	300 volts
EV Battery Rated Capacity	30.2kWh

**Table 3** Truth Table of 4 Level Input Priority Encoder

4*2 Priority Encoder Input				4*2 Priority Encoder Output		Tristate Buffers Input			
P <sub>3</sub>	P <sub>2</sub>	P <sub>1</sub>	P <sub>0</sub>	O <sub>2</sub>	O <sub>1</sub>	C <sub>3</sub>	C <sub>2</sub>	C <sub>1</sub>	C <sub>0</sub>
0	0	0	0	X	X	0	0	0	0
0	0	0	1	0	0	0	0	0	1
0	0	1	X	0	1	0	0	1	1
0	1	X	X	1	0	0	1	1	1
1	X	X	X	1	1	1	1	1	1

1: Logic High X: Don't Care; 0: Logic Low

$$\text{So, } V_o = DV_{IN} \tag{2}$$

Let's substitute the value of the  $V_{IN}$  and  $V_O$  in Eq. (2) to calculate the duty cycle of the DC-DC Converter:

$$D = \frac{V_o}{V_{IN}} = \frac{300}{480} = 0.625 \tag{3}$$

The output power of the DC-DC buck convertor for the resistive load (R) can be calculated as:

$$P = \frac{V_o^2}{R} \tag{4}$$

The value of R, L, C parameters of the DC-DC buck converters can be calculated as:

$$\text{Resistance (R)} = \frac{V_o^2}{P} = \frac{300 \times 300}{12000} = 7.5\Omega \tag{5}$$

$$\text{Inductor(L)} = \frac{(1-D)R}{2f} = \frac{(1-0.625) \times 7.5}{2 \times 25 \times 10^3} = 56.25\mu H \tag{6}$$

$$C = \frac{(1-D)}{8L \left(\frac{\Delta V_o}{V_o}\right)^2} = \frac{1-0.625}{8 \times 56.25 \times 10^{-6} \times 0.01 \times (25 \times 10^3)^2} = 133\mu F \tag{7}$$

### Mathematical Modelling of Buck Converter

The model of power circuit of buck converter is shown in Fig. 3. All parameters are considered while designing the converter for the required operation. It is also assumed that the converter is in continuous conduction mode (CCM) with duty D and switching frequency  $F_{SW} = 25$  kHz (assumed). As bus voltage i.e., source voltage ( $V_{IN}$ ) is at higher potential than the battery voltage Table 2. The objective of state space modelling is to get the transfer function equation of the buck converter which can be incorporated to tune PI controller which can be used for switching of semiconductor switch

included in the device. In CCM two modes of buck converter are discussed below.

**Case (a) Switch ON [ $0 < t < DT$ ]:** When the switch is turned on, the input voltage source serves as the circuit's power supply. Therefore, the voltage equation can be calculated as:

$$V_{IN}(t) = L \frac{di_L(t)}{dt} + \frac{RV_C(t)}{R+R_C} + \left( r_{sw} + r_L + \frac{Rr_C}{R+r_C} \right) i_L(t) \tag{8}$$

The current state variable of the inductor can be obtained by rewriting Eq. (8) as:

$$\frac{di_L(t)}{dt} = - \frac{\left( r_{sw} + r_L + \frac{Rr_C}{R+r_C} \right)}{L} i_L(t) - \frac{R}{(R+r_C)L} V_C(t) + \frac{1}{L} V_{IN}(t) \tag{9}$$

Applying KCL in Fig. 3 we get,

$$\frac{R}{R+r_C} i_L(t) = C \frac{dV_C(t)}{dt} + \frac{V_C(t)}{R+r_C} \tag{10}$$

Rewriting Eq. (10) as follows gives the inductor's voltage state variable:

$$\frac{dV_C(t)}{dt} = \frac{R}{(R+r_C).C} i_L(t) - \frac{V_C(t)}{(R+r_C).C} \tag{11}$$

The state space model of a buck converter for mode (a) can be expressed using Eqs. (9) and (11) as follows:

$$\begin{bmatrix} \frac{di_L(t)}{dt} \\ \frac{dV_C(t)}{dt} \end{bmatrix} = \begin{bmatrix} -\frac{\left( r_{sw} + r_L + \frac{Rr_C}{R+r_C} \right)}{L} & -\frac{R}{(R+r_C)L} \\ -\frac{R}{(R+r_C).C} & -\frac{1}{(R+r_C).C} \end{bmatrix} \begin{bmatrix} i_L(t) \\ V_C(t) \end{bmatrix} + \begin{bmatrix} \frac{1}{L} \\ 0 \end{bmatrix} [V_{IN}(t)] \tag{12}$$

$$A_1 = \begin{bmatrix} -\frac{\left( r_{sw} + r_L + \frac{Rr_C}{R+r_C} \right)}{L} & -\frac{R}{(R+r_C)L} \\ -\frac{R}{(R+r_C).C} & -\frac{1}{(R+r_C).C} \end{bmatrix}; B_1 = \begin{bmatrix} \frac{1}{L} \\ 0 \end{bmatrix} \tag{13}$$

A similar illustration of the buck converter output voltage for mode (a) is:

$$V_o(t) = \frac{R}{R+r_c} V_C(t) + \frac{R.r_c}{R+r_c} i_L(t) \tag{14}$$

$$V_o(t) = \begin{bmatrix} \frac{R.r_c}{R+r_c} & \frac{R}{R+r_c} \end{bmatrix} \begin{bmatrix} i_L(t) \\ V_C(t) \end{bmatrix} + [0][V_{IN}(t)] \tag{15}$$

$$C_1 = \begin{bmatrix} \frac{R.r_c}{R+r_c} & \frac{R}{R+r_c} \end{bmatrix}; \quad D_1 = [0] \tag{16}$$

**Case (b): Switch OFF [DT < t < T]:** The diode stays in the forward biased mode while the switch is OFF. Therefore, the load and inductor circuit caused the capacitor to discharge. For this mode, the voltage and current equations are as follows:

$$\frac{R}{R+r_c} V_C(t) = \left( r_D + r_L + \frac{R.r_c}{R+r_c} \right) i_C(t) + L \frac{di_L(t)}{dt} \tag{17}$$

The state variable of inductor current for mode (b) can be achieved by rewriting the Eq. (17) as:

$$\frac{di_L(t)}{dt} = -\frac{R.V_C(t)}{(R+r_c)L} - \frac{\left( r_D + r_L + \frac{R.r_c}{R+r_c} \right)}{L} i_L(t) \tag{18}$$

$$i_L(t) = i_C(t) + i_R(t) \tag{19}$$

$$C \frac{dV_C(t)}{dt} = \frac{R}{R+r_c} i_L(t) - \frac{V_C(t)}{R+r_c} \tag{20}$$

Rewriting Eq. (20) as follows yields the state variable of capacitor voltage for mode (b).

$$\frac{dV_C(t)}{dt} = \frac{R}{C(R+r_c)} i_L(t) - \frac{1}{C(R+r_c)} V_C(t) \tag{21}$$

Using Eqs. (18) and (20), the state space model of a buck converter for mode (b) can be written as follows:

$$\begin{bmatrix} \frac{di_L(t)}{dt} \\ \frac{dV_C(t)}{dt} \end{bmatrix} = \begin{bmatrix} -\frac{(r_D+r_L+R.r_c)}{(R+r_c)L} & -\frac{R}{(R+r_c)L} \\ -\frac{R}{(R+r_c)L} & -\frac{1}{(R+r_c)L} \end{bmatrix} \begin{bmatrix} i_L(t) \\ V_C(t) \end{bmatrix} + \begin{bmatrix} 0 \\ 0 \end{bmatrix} [V_{IN}(t)] \tag{22}$$

The DC-DC buck converter's output voltage can be expressed as:

$$V_o(t) = \begin{bmatrix} \frac{R.r_c}{R+r_c} & \frac{R}{R+r_c} \end{bmatrix} \begin{bmatrix} i_L(t) \\ V_C(t) \end{bmatrix} + [0][V_i(t)] \tag{23}$$

$$A_2 = \begin{bmatrix} -\frac{(r_D+r_L+R.r_c)}{(R+r_c)L} & -\frac{R}{(R+r_c)L} \\ -\frac{R}{(R+r_c)L} & -\frac{1}{(R+r_c)L} \end{bmatrix} \tag{24}$$

$$B_2 = \begin{bmatrix} 0 \\ 0 \end{bmatrix}; \quad C_2 = \begin{bmatrix} \frac{R.r_c}{R+r_c} & \frac{R}{R+r_c} \end{bmatrix}; \quad D_2 = [0] \tag{25}$$

The average value of  $A_{avg}$ ,  $B_{avg}$ ,  $C_{avg}$ , and  $D_{avg}$ , can be calculated as:

$$A_{avg} = A_1 D + A_2 (1 - D) \tag{26}$$

$$B_{avg} = B_1 D + B_2 (1 - D) \tag{27}$$

$$C_{avg} = C_1 D + C_2 (1 - D) \tag{28}$$

$$D_{avg} = D_1 D + D_2 (1 - D) \tag{29}$$

After substituting the value of  $A_1$  from Eq. (13) and  $A_2$  from Eq. (24) in Eq. (26), we get the average value  $A_{avg}$  as:

$$A_{avg} = \begin{bmatrix} -\frac{(r_{sw}+r_L+\frac{R.r_c}{R+r_c})}{L} & -\frac{R}{(R+r_c)L} \\ -\frac{R}{(R+r_c)L} & -\frac{1}{(R+r_c)L} \end{bmatrix} \tag{30}$$

After substituting the value of  $B_1$  from Eq. (13) and  $B_2$  from Eq. (25) in Eq. (27), we get the average value  $B_{avg}$  as:

$$B_{avg} = \begin{bmatrix} \frac{1}{L} \\ 0 \end{bmatrix} \tag{31}$$

After substituting the value of  $C_1$  from Eq. (16) and  $C_2$  from Eq. (25) in Eq. (28), we get the average value  $C_{avg}$  as

$$C_{avg} = \begin{bmatrix} \frac{R.r_c}{R+r_c} & \frac{R}{R+r_c} \end{bmatrix} \tag{32}$$

After substituting the value of  $D_1$  from Eq. (16) and  $D_2$  from Eq. (25) in Eq. (29), we get the average value  $D_{avg}$  as

$$D_{avg} = 0 \tag{33}$$

So, the transfer function of buck converter is as follows:

$$G_{B1}(s) = \frac{5128.21s + 128526444.43}{s^2 + 9469.93s + 131782447.47} \tag{34}$$

### Tuning of PI Controller

Transfer function equation of PI controller is as follows:

$$G_C(s) = K_p + \frac{K_i}{s} \tag{35}$$



The characteristics equation of closed loop system is given by:

$$1 + e^{-j\theta} T_1(s) \times G_C(s) = 0 \tag{36}$$

where,  $e^{-j\theta} = \cos\theta - j\sin\theta$  (37)

Putting Eq. (35) and (37) in Eq. (36), we get:

$$1 + (\cos\theta - j\sin\theta) \times \frac{b_1s + b_0}{a_2s^2 + a_1s + a_0} \left( K_p + \frac{K_i}{s} \right) = 0 \tag{38}$$

Substituting  $s=j\omega$  in Eq. (38) we get,

$$(K_p X_1 + K_i X_2) + j(K_p X_4 + K_i X_5) = X_3 + jX_6 \tag{39}$$

Here,

$$X_1 = b_0\omega\sin\theta - b_1\omega^2\cos\theta \tag{40}$$

$$X_2 = b_0\cos\theta - b_1\omega\sin\theta \tag{41}$$

$$X_3 = a_1\omega^2 \tag{42}$$

$$X_4 = b_1\omega^2\sin\theta + b_0\omega\cos\theta \tag{43}$$

$$X_5 = b_1\omega\cos\theta - b_0\sin\theta \tag{44}$$

$$X_6 = a_2\omega^3 - a_0\omega \tag{45}$$

Separating real and imaginary part in Eq. (39) We get,

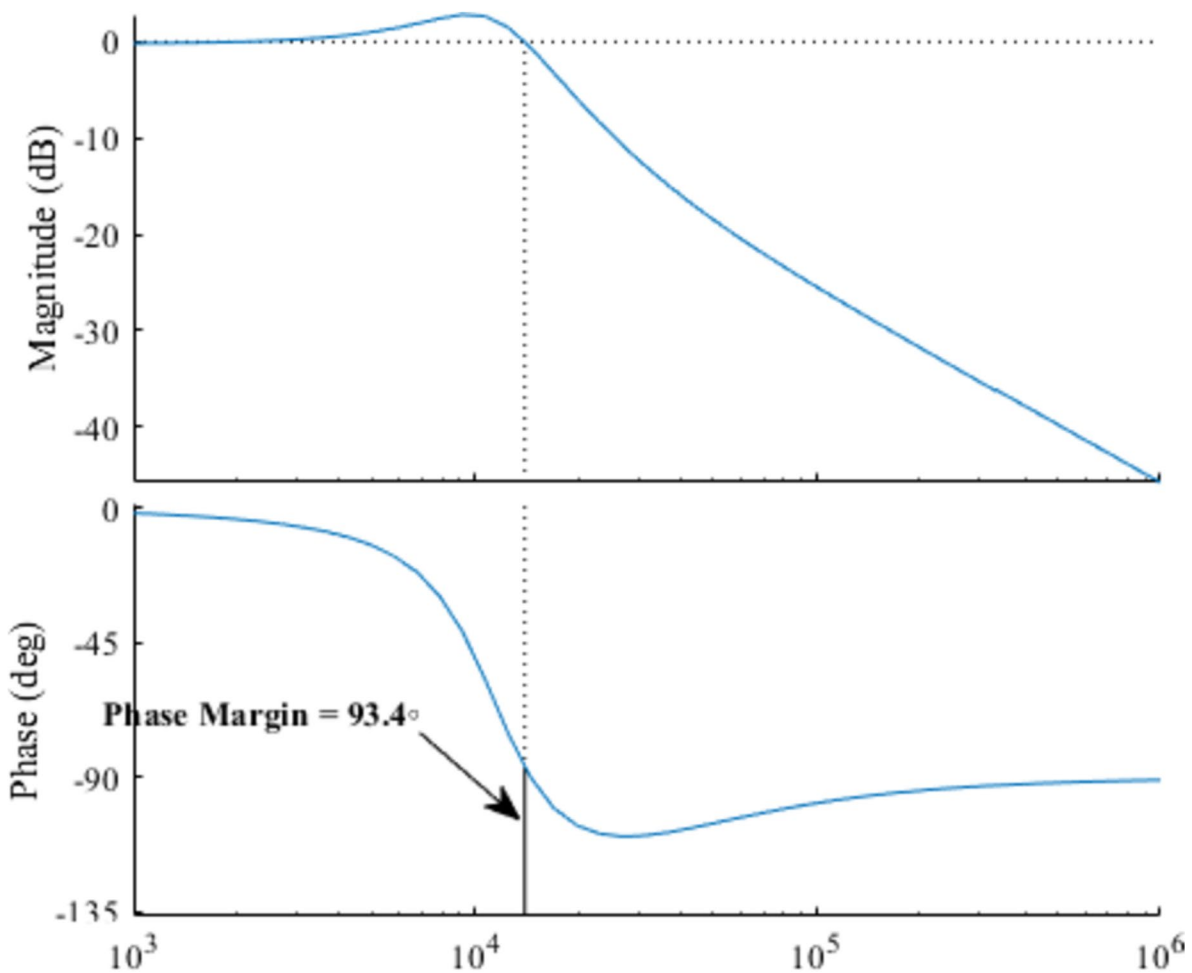
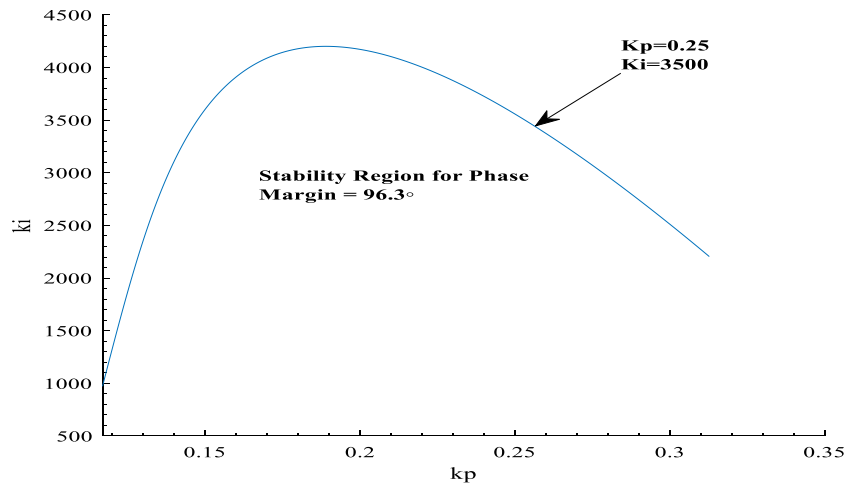


Fig. 4 Bode plot of designed buck converter

**Fig. 5** Stability Boundary Locus Plot



$$K_p(\omega, \theta) = \frac{[-a_2 b_1 \omega^3 \sin \theta + (-a_2 b_0 + a_1 b_1) \omega^2 \cos \theta + (-a_1 b_0 + a_0 b_1) \omega \sin \theta + a_0 b_0 \cos \theta]}{-(b_1^2 \omega^2 + b_0^2)} \tag{46}$$

$$K_i(\omega, \theta) = \frac{\omega \left[ \begin{matrix} -a_2 b_1 \omega^3 \cos \theta + (a_2 b_0 - a_1 b_1) \omega^2 \cos \theta \\ + (-a_1 b_0 + a_0 b_1) \omega \cos \theta - a_0 b_0 \sin \theta \end{matrix} \right]}{-(b_1^2 \omega^2 + b_0^2)} \tag{47}$$

For a required phase margin of 93.4° (Refer Fig. 4),  $K_p$  versus  $K_i$  plot at varying frequency from  $10^3$  rad/sec to  $0^4$  rad/sec is obtained as shown below. From the plot (Refer Fig. 5) it is concluded that for system to be stable for  $0.1 < K_p < 0.6$  and  $1000 < K_i < 5500$ . To tune the controller  $K_p=0.4$  and  $K_i=5000$  is considered.

We have selected  $K_p = 0.4$ ,  $K_i = 5000$ . The frequency response of the adjusted buck converter (see Fig. 6) confirms that the phase margin has been raised to 102°. This greater

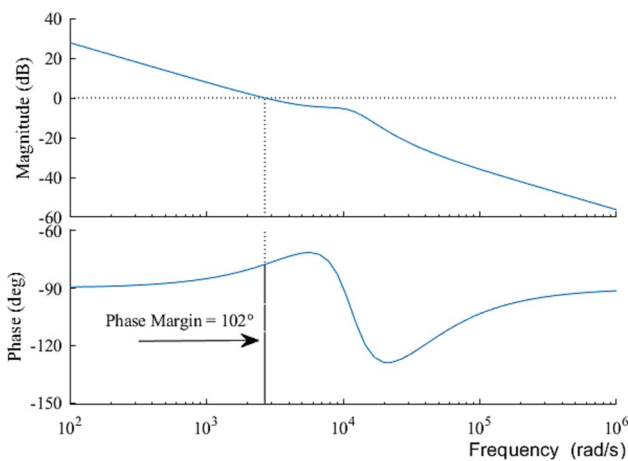


**Fig. 6** Frequency Response of PI Controlled Buck Converter

phase margin aids in preventing overshoot and hence provides system stability.

### Control Strategy of Designed Interleaved Multi-Phase Buck Converter

PI: Transfer function of outer loop proportional integral controller,  $PI_1, PI_2, PI_3,$  and  $PI_4$ : Transfer function of inner loop Phase 1, 2, 3 and 4 proportional integral controllers

$G_{B1}, G_{B2}, G_{B3},$  and  $G_{B4}$ : Transfer function of buck converter for Phase 1, 2, 3 and 4

$P_0, P_1, P_2, P_3$ : Priorities for different levels of charging

$C_0, C_1, C_2,$  and  $C_3$ : Control signals to activate the tristate buffer for different charging levels

$T_1, T_2, T_3,$  and  $T_4$ : Tristate buffers

PWM: Pulse Width Modulated Signal Generator

The control block diagram of a multi-phase buck converter (refer to Fig. 7) shows that it comprises of four buck converters coupled in parallel to accomplish interleaving. The proposed control strategy uses the converter output voltage ( $V_o$ ) as feedback and compares it to the reference voltage ( $V_{REF}$ ) to generate an error signal i.e.,  $e(t)$  for the PI controller tuned using the stability locus approach. The output generated by outer loop PI controller is in terms of reference current. The inner loop of proposed controller is divided into 4 different phases, for each phase inductor current i.e.,  $I_{L1}, I_{L2}, I_{L3}$  and  $I_{L4}$  is used as the feedback which is compared it to the reference current ( $I_{REF}$ ) generated by output of outer loop PI controller. The actuating signal generated at each phase is provided to inner loop PI Controllers. Outputs of inner loop PI controllers are provided to PWM generator to generate a gate pulse which controls the switching



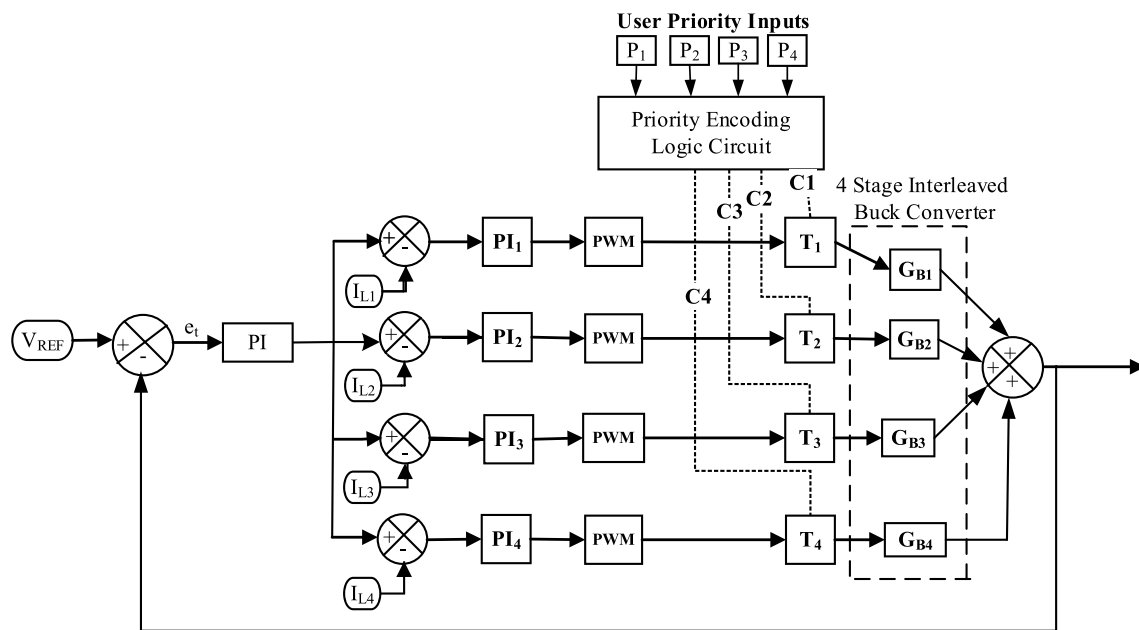
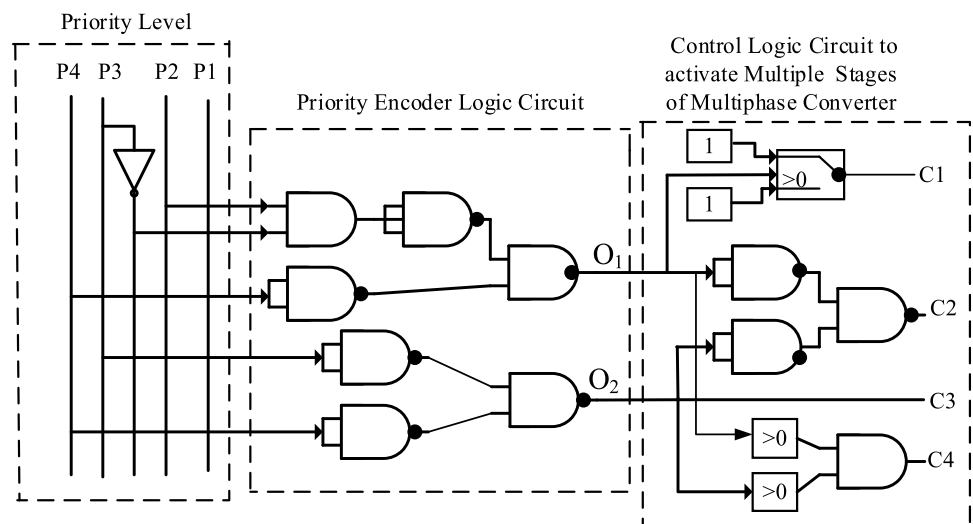


Fig. 7 Schematic Representing switching controller of Interleaved Converter

Fig. 8 Schematic Representing 4 level input priority logic combinational circuit



of MOSFETs to achieve buck operation for the respective phases. The designed converter (refer Fig. 2) is controlled by interleaved switching control i.e., gate pulses generated to activate MOSFETs have equal switching frequency but variable phase difference with an angle difference of  $90^\circ$ .

The basic idea to implement four buck converters in parallel is to achieve level 1 to level 4 charging stages in a single charging port to fulfil the objective of universal charging port. For instance, during level 1 charging phase 1 of the converter will be activated, during level 2 charging, phase

1 and 2 of buck converter (refer Fig. 7) will be activated, similarly during level 3 charging, phase 1, 2, and 3 of buck converter (refer Fig. 7) will be incorporated, similarly during level 4 all 4 phases will be activated. The level of charging will be set by the user which is based on the priority set by the EV consumer. Priority encoding logic circuit (Refer Fig.) is designed in order to generate control signals to activate the required phases for the desired output in terms of charging rate. The combinational logic circuit is incorporated using  $4 \times 2$  priority encoder along with  $2 \times 4$  digital logic circuit

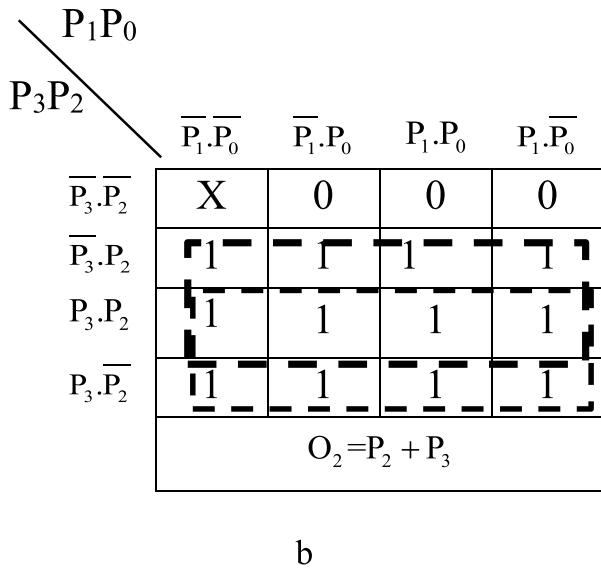
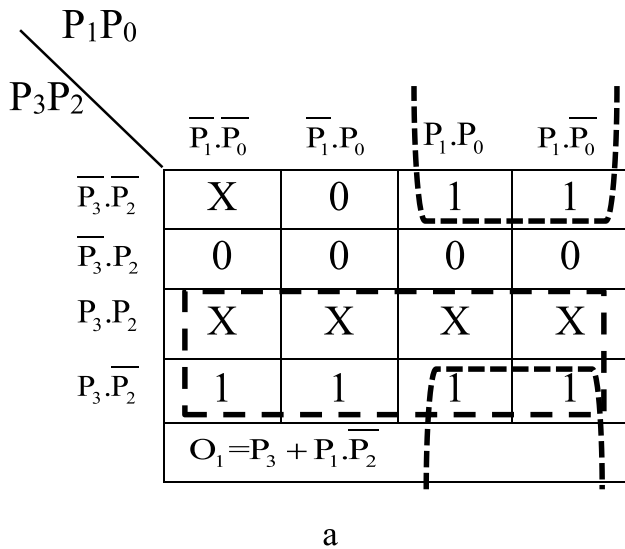


Fig. 9 (a) K-map for 4\*2 priority encoder output  $O_1$ . (b) K-map for 4\*2 priority encoder output  $O_2$

(Refer Fig. 8). The digital circuit is designed using K-map approach based on truth table (Refer Table 3) of the required circuit.

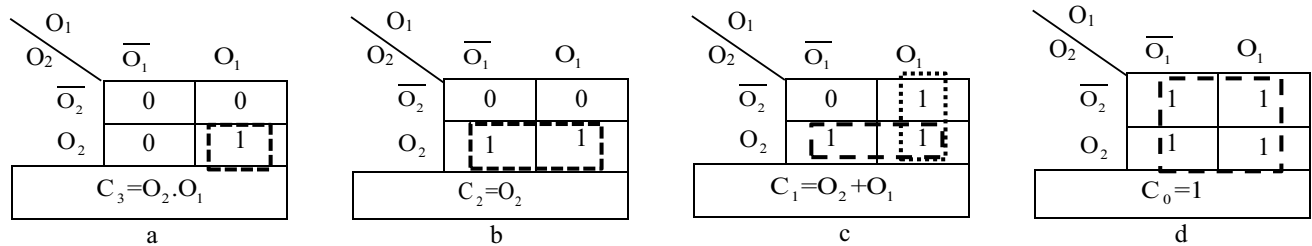


Fig. 10 (a) Boolean function for  $T_1$ . (b) Boolean function for  $T_2$ . (c) Boolean function for  $T_3$ . (d) Boolean function for  $T_4$

The proposed encoder circuit compresses the 4bit input provided by the consumer into a 2bit binary output, encoded signal is then decoded by a 2\*4 decoder to generate a 4bit output in terms of control pulses to activate tristate buffer which in turn will activate the different phases of converter.  $O_1$  and  $O_2$  are the outputs (refer Fig. 8) of the intermediate input/outputs for the digital logic circuit of the multi-phase interleaved buck converter. The  $C_0, C_1, C_2$  and  $C_3$  are output of the digital logic circuit to activate the tristate switch  $T_1, T_2, T_3$ , and  $T_4$  to operate the multi-phase interleaved buck converter at various charging levels (i.e., level 1, level2, level 3 and level 4). The K-map technique is used to obtain the digital logic diagram of the control circuit from the truth table [refer Table 3]. The K-map from the truth table [refer Table 3] for the 4\*2 priority encoder outputs  $O_2$  and  $O_1$  are shown in Fig. 9a and b. After solving K-maps, we get the Boolean expression for  $O_1$  and  $O_2$  as shown in Fig. 9a and b respectively.

From the truth table (refer Table 3), we obtain the K-map and Boolean expression for tristate input of the switches ( $T_1, T_2, T_3$  and  $T_4$ ) in term of outputs  $O_2$  and  $O_1$  respectively in Fig. 10a, b, c and d as below. The Boolean function of tristate switch ( $T_4$ ) input ( $C_3$ ) can be calculated using as:

$$C_3 = O_2.O_1 = (P_2 + P_3).(P_3 + P_1.\overline{P_2})$$

$$= P_2P_3 + P_3 + P_3P_1.\overline{P_2} = P_3(1 + P_1.\overline{P_2}) = P_3 \tag{48}$$

The Boolean function of tristate switch ( $T_3$ ) input ( $C_2$ ) can be calculated using as:

$$C_2 = O_2 = P_2 + P_3 \tag{49}$$

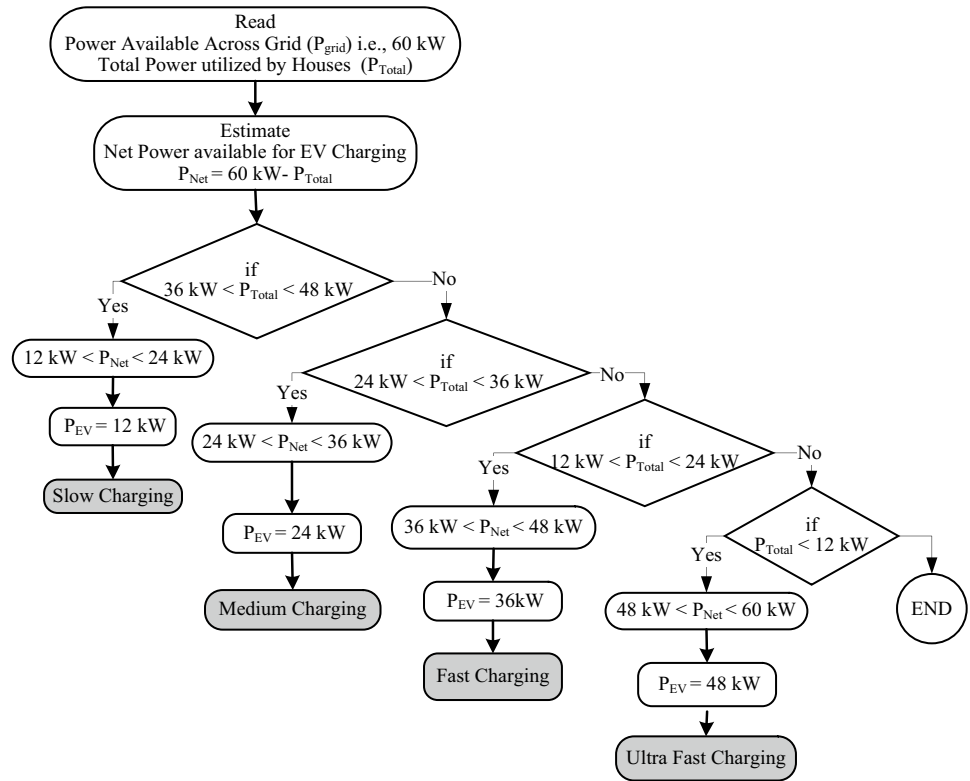
The Boolean function of tristate switch ( $T_2$ ) input ( $C_1$ ) can be calculated using as:

$$C_1 = O_2 + O_1 = (P_2 + P_3) + (P_3 + P_1.\overline{P_2}) = P_2 + P_3 + P_1.\overline{P_2} \tag{50}$$

The Boolean function of tristate switch ( $T_1$ ) input ( $C_0$ ) can be calculated using as:

$$C_0 = 1 \tag{51}$$

**Fig. 11** Flow Chart representing of the proposed algorithm



**Analysis of Proposed Algorithm**

The flow chart of the priority-based control algorithm is shown in Fig. 11. The battery capacity of electric vehicle is 32.2 kWh and 100 Ah (considered) for this case study. There are four modes considered to test the performance of the proposed algorithms. Priority-based optimization is used to keep the grid power level upto 60kW. In this mode:

$$P_{Net} = P_{grid} - P_{Total} \tag{52}$$

$$P_{EV} = P_{Net(L)} \tag{53}$$

$P_{Net(L)}$  is the lower rate power from net power.

The charging time of the electric vehicle can be calculated as:

$$T_c = \frac{\mu_{EV}}{I_c} \tag{54}$$

where  $T_c$  is charging time of electric vehicle,  $\mu_{EV}$  is the battery capacity of electric vehicle,  $I_c$  is the charging current of electric vehicles.

**Case 1 (Priority-Low Charging):** When power consumed by the houses across the community lies between 36-48 kW then based on the proposed algorithm (refer Fig. 11) remaining power across the grid which is maintained at 60

kW will be in the range of 12-24 kW and this will operate the charger with low priority ( $P_0$ ) at that instant the priority encoder input will be 0001 (Refer Table 3). The digital control logic circuit (refer Fig. 8) generate a control signal 0001 (i.e., only  $C_0$  will be high) to activate the tristate buffers. Therefore, only tristate buffer  $T_1$  will remain high and multi-phase interleaved converter will charge the electric vehicle at level 1 of average output current of 40 amp (refer Fig. 13) at 300 volts.

In this mode, the charging current is 40 A, the charging time of the electric vehicle can be estimated as:

$$T_c = \frac{100 \text{ Ah}}{40 \text{ A}} = 2.5 \text{ Hours or } 150 \text{ minutes}$$

Therefore, the multi-phase interleaved buck converter charges the electric vehicle with average power of 12 kW in this mode and electric vehicle of 30.2 kWh battery will fully charge within 150 minutes. In this mode:

$$P_{Net} = 60 - (36 \text{ to } 48) \text{ kW}$$

$$P_{Net} = 12 \text{ kW to } 24 \text{ kW}$$

$$P_{EV} = 12 \text{ kW}$$

So, to adopt the slow charging rate to balance the grid power upto 60 kW.

**Case 2 (Priority-Medium Charging):** When power consumed by the houses across the community is between 24-36Kw then based on the proposed algorithm remaining power across the grid will lie between 24-36 kW. This will lead to operation of charger at medium priority ( $P_1$ ) at that instant the priority encoder input will be 0010 (Refer Table 3). The digital control logic circuit (refer Fig. 8) generate a control signal 0011 (i.e., only  $C_1$  and  $C_0$  will be high) to activate the tristate buffers. Therefore, only tristate buffers  $T_1$  and  $T_2$  will remain ON, and multi-phase interleaved converter will charge the electric vehicle at level 2 (Medium) of average output current of 80 amp (refer Fig. 14) at 300 volts.

In this mode, the charging current is 80 A, the charging time of the electric vehicle can be estimated as:

Therefore, the multi-phase interleaved buck converter charges the electric vehicle with average power of 24 kW in this mode and electric vehicle of 30.2 kWh battery will fully charge within 75 minutes. In this mode:

$$P_{Net} = 60 - (24 \text{ to } 36)\text{kW}$$

$$P_{Net} = 24 \text{ kW to } 36 \text{ kW}$$

$$P_{EV} = 24 \text{ kW}$$

So to adopt the medium charging rate to balance the grid power upto 60 kW.

**Case 3 (Priority-Fast Charging):** When overall Power consumed by all the houses across the community is between 12-24 kW then remaining power that will be utilized by the charger will lie between 36-48kW. This will lead to operation of charger at Fast Charging priority ( $P_2$ ) at that instant the priority encoder input will be 0100 (Refer Table 3). The digital control logic circuit (refer Fig. 8) generate a control signal 0111. It means the  $C_2$ ,  $C_1$  and  $C_0$  will be high and  $C_3$  will remain at low state. Therefore, tristate buffers  $T_1$ ,  $T_2$  and  $T_3$  will remain ON, while tristate buffer remains on OFF state. So, the multi-phase interleaved converter will charge the electric vehicle at level 3 (Fast Charging) of average output current of 120 amp (refer Fig. 14) at 300 volts. In this mode, the charging current is 120 A, the charging time of the electric vehicle can be estimated as:

$$T_c = \frac{100\text{Ah}}{120\text{A}} = 0.83 \text{ Hours or } 50 \text{ minutes}$$

Therefore, the multi-phase interleaved buck converter charges the electric vehicle with average power of 36 kW in this mode and electric vehicle of 30.2 kWh battery will fully charge within 50 minutes. In this mode:

$$P_{Net} = 60 - (12 \text{ to } 24) \text{ kW}$$

$$P_{Net} = 36 \text{ kW to } 48 \text{ kW}$$

$$P_{EV} = 36 \text{ kW}$$

So to adopt the fast charging rate to balance the grid power upto 60kW.

**Case 4 (Priority-Ultra Fast Charging):** In this case power consumed by the houses across the community is less than 12kW then remaining power as per the proposed algorithm will be operated at rating greater than 48kW and at this instant the priority level will be superfast charging i.e.,  $P_4$ . The digital control logic circuit (refer Fig. 8) generate a control signal 1111. It means the  $C_2$ ,  $C_1$  and  $C_0$  and  $C_3$  will be high. Therefore, tristate buffers  $T_1$ ,  $T_2$ ,  $T_3$  and  $T_4$  will remain ON. So, the multi-phase interleaved converter will charge the electric vehicle at level 4 (Super-Fast Charging) of average output current of 160 amp (refer Fig. 15) at 300 volts. Therefore, the multi-phase interleaved buck converter charges the electric vehicle with average power of 48 kW in this mode and electric vehicle of 30.2 kWh battery will fully charge within 37.5 minutes.

In this mode, the charging current is 160 A, the charging time of the electric vehicle can be estimated as:

The main objective behind the control strategy is to provide a cost and energy effective solution to electric vehicle consumer in terms of battery charging current to charge EV battery with up to 4 charging modes (Refer Table 4) based on availability of power across grid. As shown in Table 4, the charging time of a 30-kW electric vehicle for four different priorities is estimated. During low priority ( $P_0$ ) then a 30.2 kWh electric vehicle charge 100 percentage within 150 minutes, during ultra-fast charging priority the 30.2 kWh electric vehicle will charge at 4 times faster rate as compare the charging with low priority and charge 100 percent within 37.5 minutes as mentioned in Table 4.

In this mode:

**Table 4.** Battery Charging Time and Current based on EV Consumer Input

EV Consumer Priority Input	Priority Encoder Output	Charging Current (Ampere)		30 kW Electric Vehicle Charging Time (Minutes)
		$O_2$	$O_1$	
Low	$P_0$	0	0	150
Medium	$P_1$	0	1	75
Fast	$P_2$	1	0	50
Ultra-Fast	$P_3$	1	1	37.5

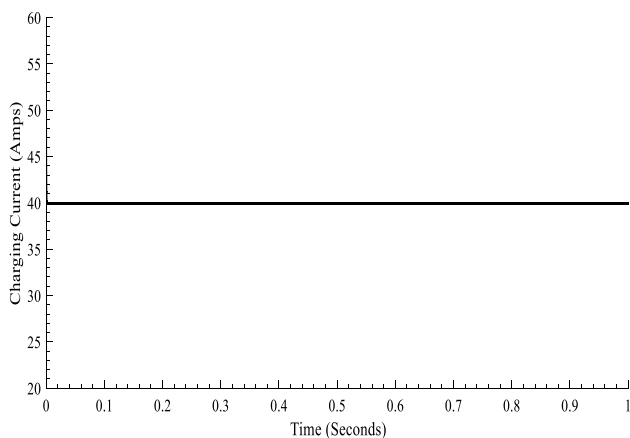


Fig. 12 Charging Current during level 1 Charging mode

$$P_{Net} = 60 - (12)kW$$

$$P_{Net} = 48kW$$

$$P_{EV} = 48kW$$

So, to adopt the ultra-fast-charging rate to balance the grid power upto 60kW.

**Note:** The charging current curves represented in Figs. 12, 13, 14 and 15 are extracted during simulation performed out with the designed Universal Interleaved EV charger, driving the variable loads within the operational range of charger i.e., 12-48 kW.

The cost analysis for electric vehicles (EVs), involves several factors, including peak and off-peak electricity rates, charging efficiency, and overall energy costs. Utility companies have tiered pricing for electricity, with higher rates during peak hours. Charging during peak hours can significantly increase the costs. Off-peak rates are typically lower and occur during times of lower electricity demand. Charging during off-peak hours can help save on electricity costs.

Fig. 13 Charging Current during level 2 Charging mode

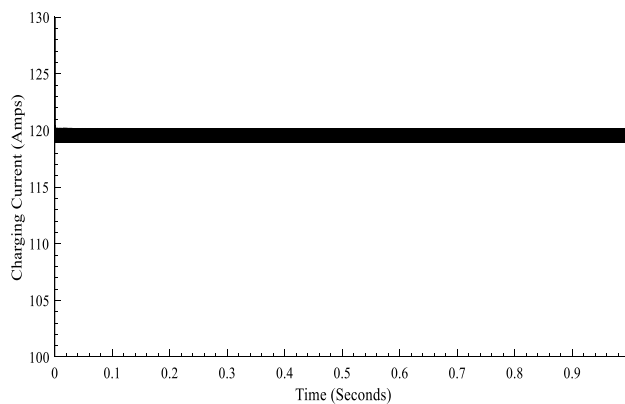
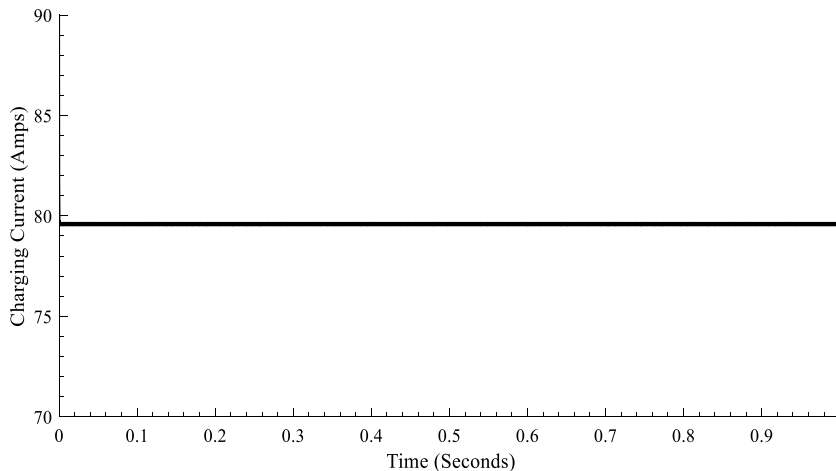


Fig. 14 Charging Current during level 3 Charging Mode

The efficiency of the charging process can impact the amount of electricity user need to charge the EV. Some energy is lost as heat during the charging process. The charging efficiency varies depending on the charger type (e.g., Level 1, Level 2, DC fast charging). The time it takes to charge the EV affects the cost. Faster charging methods like DC fast charging may be more expensive per kilowatt-hour but can save time. EV's battery capacity plays a role in the overall cost. A larger battery will require more electricity to reach a full charge, increasing your costs. Calculating the overall energy cost involves considering the electricity rates, charging efficiency, and the energy capacity of your EV's battery. The formula to calculate cost is:

$$C = (\eta_c \times C_B) \times R \tag{55}$$

where, C is Cost,  $\eta_c$  is Charging Efficiency,  $C_B$  is battery capacity and R is electricity rate.

In this scenario, you can see that charging during off-peak hours is more cost-effective.

**Fig. 15** Charging Current during level 4 Charging Mode

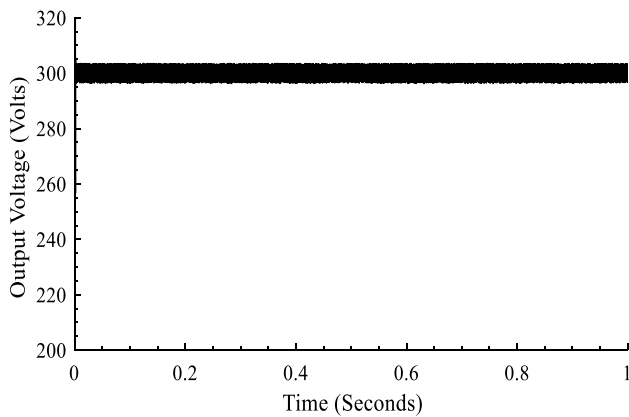
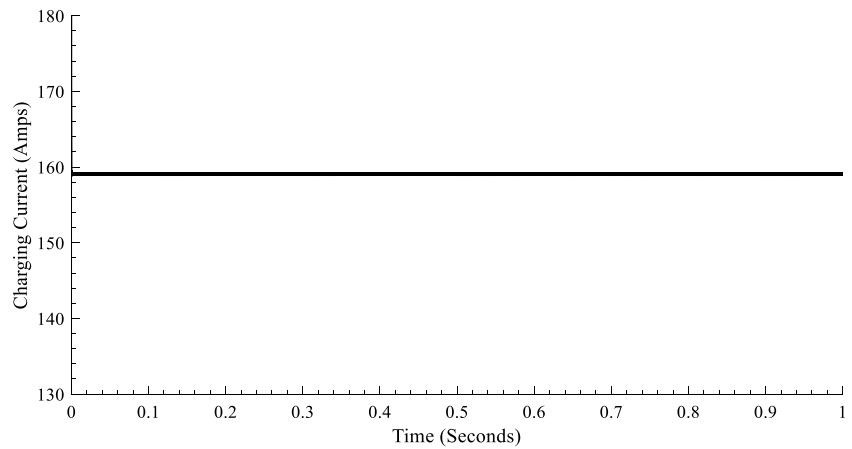


**Fig. 16** Output Voltage curve of multi-stage interleaved buck converter

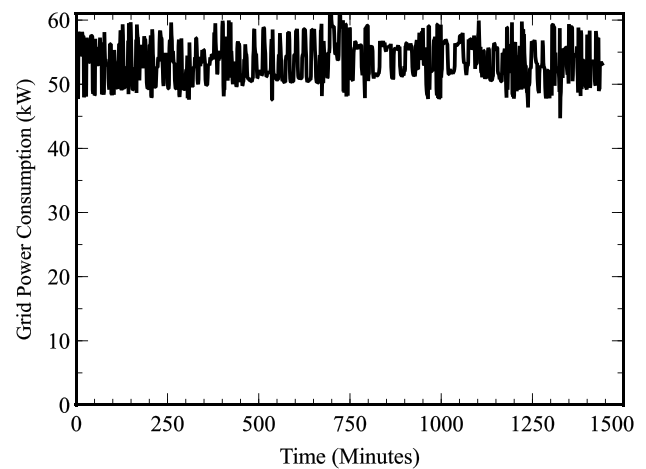


**Fig. 17** Power consumption from grid

## Simulation Results

This section serves to analyze the way the multi-phase interleaved universal charger that was created using the suggested algorithm performs. The algorithm's main goal is to use the EV charger as efficiently as possible given the amount of power still available on the grid. Using Simulink, a MATLAB-based graphical programming environment for modelling, simulating, and analyzing multidomain dynamical systems, a real-time application based on the suggested technique has been simulated. All simulations provided in this research were run on a computer based on AMD Ryzen® 7, 6800H CPU 3.2GHz with 16 GB RAM operated with Microsoft Windows 11 Edition 64-bit operating system.

The performance of PI controller designed to achieve proper buck operation is also verified in this section. The control strategy for buck converter and tuning of PI controller using graphical approach is described in previous sections. To analyze that PI controller is tuned perfectly voltage curve is obtained and based on Fig. 16 it is determined that output voltage is regulated at desired level of

300V. From Fig. 11, it has been verified that tuned PI controller is able to maintain due to load variations from  $3\Omega$ - $12\Omega$ .

Actual load consumption data from domestic households have been considered to create and validate the system with great accuracy and precision. To operate grid at maximum efficiency (refer Fig. 17) once the load demand across households is met the remaining power is utilized by the EV charger to maintain grid at constant level.

As shown in figure Fig. 18 from 0-750 minutes the load consumed by the household lies within the range of 0-10 kW whereas from 750-1440 minutes load demand increases to 20 kW. The proposed method during first phase (0-750 minutes) operates a charger at ultra-fast charging mode i.e., in the range of 40-50kW (Refer Fig. 19). Similarly, during second phase (750-1440 minutes) load demand across the household is increased and to maintain power across the grid for its stability EV charger get switched into Fast Charging mode i.e., 30-40 kW (refer Fig. 19).



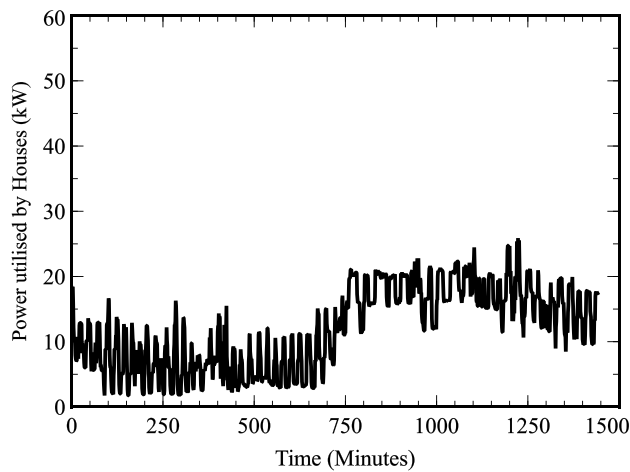


**Fig. 18** Power utilized by households within community of various EV users

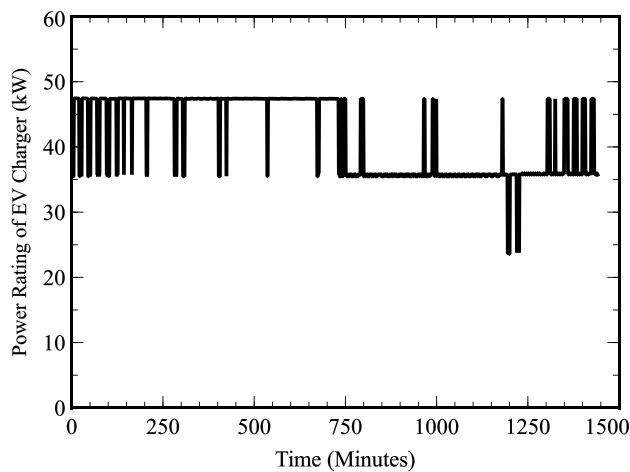


**Fig. 19** Power utilized by EV charger for power balancing in Grid

In automatic selection the user need not to bother about the switching the electric vehicle charging mode according to the peak load and grid supply, it will automatically select by the priority checker. However, if there is requirement of charge the vehicle in fast mode during urgency then the manual mode will be helpful but there is more swathing delay due to this.

With proper planning, investment, and a commitment to standardization, it is feasible to develop a reliable and accessible EV charging infrastructure to support the growing adoption of electric vehicles. Public-private partnerships and government support can play a significant role in making this transition smoother and more efficient. At initial stage it can be implemented in house and in offices.

## Conclusion

This paper describes a 3-phase AC grid-interfaced universal electric car charger based on DC-DC interleaved buck converters. The paper provides a detailed mathematical analysis of the system, considering non-idealities in the converter elements, to create a precise mathematical representation of the suggested system. The transfer function equation of the system is derived, and the stability of the system is estimated, which shows that the system is not stable. To stabilize the system, a PI-based controller is used, and the controller's parameters are tuned using stability boundary locus technique. The proposed system offers a degree of freedom to the user, allowing them to choose from 4 different modes of EV charging based on time, financial viability, and availability of power across the grid. The performance of the system was tested under various load scenarios, and the results show that the DC bus voltage is always regulated to the desired value, and a variable charging rate is produced by varying the charging current's amplitude. The proposed system can be utilized to maintain grid stability, and the same procedure can also be followed for microgrid configurations. The aim of the proposed algorithm is to provide economic viability along with a degree of freedom in terms of EV charging rate, making the system less complicated and more user-friendly. In future it can be integrated with renewable energy resources like solar and wind. In that case the load curve will be shifted, and off-peak and peak hours will change.

The proposed multi-phase interleaved universal charging port faces a significant drawback due to its reliance on a consistent electric grid. This limits its suitability in remote or poorly connected areas where electricity access is sporadic, hindering widespread electric vehicle adoption. Infrastructure upgrades would be required in such regions, increasing complexity and cost. Users may experience reduced reliability, impacting the convenience of electric vehicles. In emergency situations or underserved areas, the charging port's dependence on a stable grid may pose challenges. Future solutions could involve integrating energy storage systems or designing grid-independent charging stations, enhancing accessibility and resilience in less reliable grid environments.

**Acknowledgment** This research work is financial supported by UGC-BSR Research Start-Up-Grant, University Grant Commission Government of India.

**Data Availability** My manuscript has no associated data.

## References

1. Menegaki AN, Tsagarakis KP (2015) Rich enough to go renewable, but too early to leave fossil energy? *Renew Sustain Ener Rev* 41(1):1465–1477

2. Rehman S, El-Amin IM, Ahmad F, Shaahid SM, Al-Shehri AM, Bakhashwain JM, Shash A (2007) Feasibility study of hybrid retrofits to an isolated off-grid diesel power plant. *Renew Sustain Ener Rev* 11(4):635–653
3. Progress toward sustainable energy. Global tracking framework report, pp 1–8. [Available Online: <http://trackingenergy4all.worldbank.org/~media/GIAWB/GTF/Documents/GTF-2015>]
4. World Energy Outlook 2014 Factsheet. How will global energy markets evolve to 2040, International Energy Agency, 2014. [Online Available: [http://www.worldenergyoutlook.org/media/weowebiste/2014/141112\\_WEO\\_FactnSheets.pdf](http://www.worldenergyoutlook.org/media/weowebiste/2014/141112_WEO_FactnSheets.pdf)]
5. Jeykishan KK, Kumar S, Nandakumar VS (2021) Standards for EV charging in India: a review. *Energy Storage*, Wiley. 1-19. <https://doi.org/10.1002/est.2.261>
6. Sharma A and Gupta R (2021) Bharat DC001 charging standard Based EV fast charger. In: Proc. 46<sup>th</sup> Annual Conference IEEE Conference of Industrial Application Society, Singapore. 3588-3593
7. Brenna M, Foadelli F, Leone C, Longo M (2020) Electric Vehicles Charging Technology Review and Optimal Size Estimation. *J Electric Eng Technol* 15:2539–2552
8. Amoriya V, Chauhan RK, Panit Jahanvi V, Verma S, Mittal S, Chauhan K, Upadhyay S, Cardenas A (2022) Modelling of Bidirectional Electric Vehicle Charger for Grid Ancillary Services. *Int J Emerg Electric Power Syst* 23(6)
9. Chauhan RK, Chauhan K (2019) *Distributed Energy Resources in Microgrids: Integration, Challenges and Optimization*. 1<sup>st</sup> Edition, Elsevier. 1-535
10. Chauhan K, Chauhan RK (2017) Optimization of Grid Energy using Demand and Source Side Management for DC Microgrid. *J Renew Sustain Ener* 9(3):035101–15
11. Chauhan RK, Rajpurohit BS, Wang L, Gonzalez-Longatt FM, Singh SN (2017) Real time energy management system for smart buildings to minimize the electricity bill. *Inter J Emerg Electr Power Syst*, DE GRUYTER 18(3):1–15
12. Kumar JS, Gajpal T (2016) A multi-input DC-DC converter for renewable energy applications. *Int Res J Eng Technol* 3(3):380–384
13. Mohan N, Undeland TM, Robbins WP (2003) *Power Electronics: Converters Application and Design*. 3<sup>rd</sup> ed. John Wiley
14. Thiyagarajan A, Praveen Kumar SG, Nandini A (2014) Analysis and comparison of conventional and interleaved DC/DC converter. International conference on Current Trends in Engineering and Technology, India. 198-205
15. Hegazy O, Mierlo JV, Lataire P (2008) Analysis, modelling and implementation of a multidevice interleaved DC/DC converter for fuel cell hybrid electric vehicles. *IEEE Trans Power Electron* 27(11):4445–4458
16. Forsyth AJ, Mollov SV (1998) Modelling and control of DC-DC converters. *Power Ener J* 12(5):229–236
17. Tan RHG, Hoo LYH (2015) DC-DC converter modelling and simulation using state space approach. In: Proc. IEEE Conference on Energy Conversion (CENCON), Malaysia. 42-47
18. Hanif Z, Shah SAA (2019) PID controller for DC-DC boost converter for photovoltaic power generation. *Int J Modern Res Eng Management* 2(4):7–12
19. Ramya KC, Jegathaesan V (2016) Comparison of PI and PID controlled bidirectional DC-DC converter systems. *Int J Power Electron Drive Syst* 7(1):56–65
20. Kolar JW, Drofenik U, Zach FC (1999) Vienna rectifier II-a novel single-stage high-frequency isolated three-phase PWM rectifier system. *IEEE Trans Indust Electron* 46(4):674–691
21. Kim JM, Lee J, Eom TH, Bae KH, Shin MH, Won CY (2018) Design and control method of 25 kW highly efficient EV fast charger," in *Proc. International Conference on Electrical Machines and systems*, South Korea, pp 2603-26-7
22. Baba D (2012) Benefits of a multiphase buck converter. *Analog Applications Journal Texas Instruments Incorporated*. 8-15
23. Garg MM, Hote YV, Pathak MK, Behera L(2018) An approach for buck converter PI controller design using stability boundary locus. In: Proc. IEEE/PES Transmission and Distribution Conference and Exposition. 1-5
24. Garg MM, Pathak MK, Chauhan RK (2020) Modeling and control of DC-DC converters for DC microgrid application. *Microgrids for Rural Areas: Research and Case Studies*, IET. 331-358. [https://doi.org/10.1049/pbpo160e\\_ch13](https://doi.org/10.1049/pbpo160e_ch13)
25. Zhi Y, Weiqin W, Haiyun W, Razmjoooy N (2021) New approaches for regulation of solid oxide fuel cell using dynamic condition approximation and STATCOM. *Int Trans Electric Energy Syst* 31(2):212756
26. Zhang H, Razmjoooy B(2023) Optimal elman neural network based on improved gorilla troops optimizer for short-term electricity price prediction. *J Electr Eng Technol* 1-15

**Publisher's Note** Springer Nature remains neutral with regard to jurisdictional claims in published maps and institutional affiliations.

Springer Nature or its licensor (e.g. a society or other partner) holds exclusive rights to this article under a publishing agreement with the author(s) or other rightsholder(s); author self-archiving of the accepted manuscript version of this article is solely governed by the terms of such publishing agreement and applicable law.